Double μ2-(phenoxido)-bridged dinuclear and polynuclear nickel(II) complexes: Magnetic properties and DNA/protein interaction

Aparup Paul [a], Albert Figuerola[b], Horst Puschmann[c], Subal Chandra Manna[a]

[a]*Department of Chemistry and Chemical Technology, Vidyasagar University, Midnapore 721102, West Bengal, India, E-mail: scmanna@mail.vidyasagar.ac.in, Fax: (91) (03222) 275329.*

[b] *Departament de Química Inorgànica i Orgànica (Secció de Química Inorgànica) and Institut de Nanociència i Nanotecnologia (IN2UB), Universitat de Barcelona, Martí i Franquès 1-11, 08028 Barcelona, Spain.*

[c] *Department of Chemistry, University of Durham, South Road, Durham DH1 3LE, U.K.*

ABSTRACT

One dinuclear and one 1D polymeric nickel(II) complex, namely {[Ni2(HL)2(pa)2(H2O)2]·DMF} (1) and {[Ni2(HL)2(ppda)(H2O)2]·DMF·H2O}n (2) (H2L = (E)-2-((1-hydroxybutan-2-ylimino)methyl)phenol, pa = 3-phenylacrylate, ppda = p-phenylenediacrylate) have been synthesized and characterized by X-ray single crystal structure determination. Complex 1 is double phenoxo-bridged dinuclear Ni(II) complex, whereas complex 2 is a 1D polynuclear chain where double phenoxo-bridged dinuclear units are connected through bridging ppda ligands. The variable temperature magnetic behavior of the complexes was studied using the Hamiltonian H = −JS1S2, S1 = S2 = SNi and confirms the presence of an overall antiferromagnetic interaction in both complexes. Good agreement between the experimental and simulated curves were found using the parameters: gNi = 2.15, DNi = 4.0 cm−1 and JNi–Ni = −0.60 cm−1 for 1, and gNi = 2.15, DNi = 4.8 cm−1 and JNi–Ni = −3 cm−1 for 2. The interactions of the complexes with CT-DNA were investigated using UV–Vis absorption and fluorescence spectroscopic methods and they

show that both the complexes interact with CT-DNA. The intrinsic binding constants values for interaction with CT-DNA are $3.9(\pm0.10) \times 105$ and $3.43(\pm0.09) \times 105\ M{-}1$ for 1 and 2, respectively. The interactions of the complexes with bovine serum albumins (BSA) and human serum albumins (HSA) were also studied using electronic absorption and fluorescence spectroscopic techniques and the results show that both complexes interact with the serum albumins via a ground state association process.

Keywords:

Double μ2-(phenoxido)-bridgedNi(II) complexCrystal structureMagnetic propertiesDNA/protein binding

Introduction

Schiff base coordinated 3d metal complexes are important due to their interesting structures and potential applications in various fields, e.g. magnetism [1], catalysis [2] and bioinorganic chemistry [3]. The use of combined multidentate Schiff bases and mono/poly carboxylate ligands is an important strategy for the designed and synthesis of polynuclear 3d metal coordination compounds. Schiff base ligands chelate some coordination sites, whereas carboxylate groups act as bridging ligands for the formation of polynuclear complexes. The bridging ligand plays a crucial role for the magnetic exchange interaction between paramagnetic centers in coordination compounds. Short span bridging ligands, such as phenoxo, alkoxo and azido bridges, are suitable ligands for magnetic exchange between paramagnetic centers. Combined Schiff base and short span coordinated nickel(II) complexes show interesting magnetic properties [4].

Nickel(II) complexes can effectively interact and damage DNA under physiological conditions, hence the study of the interaction of these complexes with DNA is important for developing nickel metal based pharmaceuticals [3](a), [3](b). On the other hand, serum albumin is the major soluble protein in blood plasma and functions as transporter and depositor of many compounds like pharmaceuticals and fatty acids etc. [5]. Factors such as the nature of the ligands, geometry of the metal complexes and the polarity of the complexes play important roles in the binding affinities of metal complexes with macro molecules, i.e. CT-DNA and proteins. Therefore the study of the interactions of DNA and proteins with nickel(II) complexes is important for the design and discovery of new nickel(II) metal based drugs [6]. Some nickel(II) coordination compounds that strongly bind DNA and interact with serum albumins show potential biological applications such as antitumor [7], antifungal [8], antibacterial [9], antimicrobial [10] and anticancer [11] activities. However, most of these complexes are mononuclear and only limited studied are reported on di-/poly-nuclear Ni(II) complexes [12]. A literature survey reveals that Schiff base coordinated nickel complexes are widely studied for their individual magnetic properties and biological activities [3](a), [3](b), [4], [6], [7], [8], [9], [10], [11]. However, to the best of our knowledge, to date there is no report on nickel(II) compounds with combined studies of their magnetic properties and biological activities.

Cinnamic acid and p-phenylenediacrylic acid both are multidentate aromatic carboxylic acids and contain a CC bond in the side chain. These CC bonds make the carboxylates a rigid ligand. In the present contribution we have used the multidentate chelating ligand (E)-2-((1-hydroxybutan-2-ylimino)methyl)phenol (H2L) in combination with 3-phenylacrylate (pa)/1, 4-benzenediacrylate (ppda) and have synthesized two nickel(II) complexes

{[Ni2(HL)2(pa)2(H2O)2]·DMF} (1) and {[Ni2(HL)2(ppda)(H2O)2]·DMF·H2O}n (2). The combination of H2L and pa results in a double phenoxido bridged dinuclear nickel complex, whereas the combination of H2L and ppda results in a 1D polymeric chain, where double phenoxido bridged nickel units are connected through the ppda ligand. Variable temperature magnetic measurements and the interactions of the complexes with BSA, HSA and CT-DNA have been studied.

Experimental

Materials. High purity 2-Amino-1-butanol was purchased from the Aldrich Chemical Co. Inc. and salicyldehyde from Merck India chemicals all other chemicals were of AR grade and used without further purification. Solvents used for spectroscopic studies were purified and dried by standard procedures before use.

Physical measurements. Elemental analyses (carbon, hydrogen and nitrogen) were performed using a Perkin-Elmer 240C elemental analyzer. IR spectra were recorded as KBr pellets on a Bruker Vector 22 FT IR spectrophotometer operating from 400 to 4000 cm^{-1}. ESI-MS spectra were recorded on a JEOL MS 700 mass spectrometer in fast atom bombardment (FAB) mode. NMR spectra of ligands recorded on Bruker 200 MHz instrument. Electronic absorption spectra were obtained with Shimadzu UV-1601 UV-vis spectrophotometer at room temperature. Quartz cuvettes with a 1 cm path length and a 3 cm^3 volume were used for all measurements. Emission spectra were recorded on a Hitachi F-7000 spectrofluorimeter. Room temperature (300 K) spectra were obtained in methanol solution using a quartz cell of 1 cm path length. The slit width was 2.5 nm for both excitation and emission.

The fluorescence quantum yield was determined using phenol as a reference and water [refractive index (η), 1.333)] medium for phenol. The solvent used for complexes is methanol (η, 1.329). Emission spectra were recorded by exciting the complex and the reference phenol at the same wavelength, maintaining nearly equal absorbance (~0.1). The area of the emission spectrum was integrated using the software available in the instrument and the quantum yield was calculated[13] according to the following equation:

$$1. \quad \Phi_S = \Phi_r \frac{A_s}{A_r} \frac{I_r}{I_s} \frac{\eta_s^2}{\eta_r^2}$$

Where Φ_s and Φ_r are the fluorescence quantum yield of the sample and reference, respectively. A_s and A_r are the respective optical densities at the wavelength of excitation, I_s and I_r correspond to the areas under the fluorescence curve; and η_s and η_r are the refractive index values for the sample and reference, respectively.

Synthesis of the ligand

A methanolic solution (20 mL) of mixture of 2-amino-1-butanol (0.089 g, 1 mmol) and salicyldehyde (0.122 g, 1 mmol) was refluxed for 3h. The resulting yellow colour solution cooled to room temperature and solid yellow compound was obtained after evaporation of solvent under reduced pressure. The compound obtained was redissolved in MeOH and filtered. The solution was left for slow evaporation at room temperature. After one week, yellow crystals of HL were obtained. Yield: 0.1642g (85%). *Anal.*Calc. for $C_{11}H_{15}NO_2$(193.24): C, 68.36; H,7.82; N,7.24%. Found: C,..... ; H,....; N, ... %. HR-MS: $[M + H]^+$, m/z, 194.24 (100%) calcd: m/z, 194.25. ^{1}H NMR (400 MHz, $CDCl_3$, δ ppm): 0.709-0.886 (3H, m), 1.474-1.655 (2H, m), 2.576 (1H, s), 3.466-3.690 (1H, m; 2H, m), 4.957 (1H, s), 6.823-6.921 (1H, d; 2H, m), 7.226-7.298 (1H, d; 2H, m),

8.306 (1H, s). ^{13}C NMR ($CDCl_3$, 400 MHz, δ ppm): 165.41 (Ar−C−OH), 161.71 (−CH=N−), 132.45-113.71 (Ar−C), 73.03 (-CH_2-OH), 66.23 (=N-CH-), 25.05 (-CH_2-), 10.51 (-CH_3).

Synthesis of complexes

The complexes have been synthesized by adopting the procedures schematically given in Scheme **1**.

Scheme 1. Synthesis of **1** and **2**

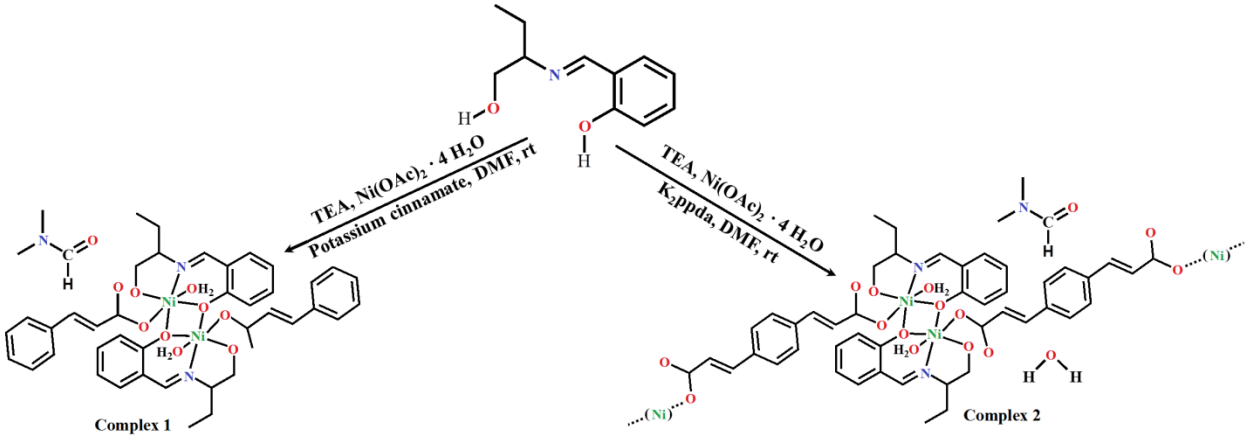

Synthesis of [{$Ni_2(L)_2(ppda)_2(H_2O)_2$}·DMF· H_2O] (1).

The methanolic solution of the ligand was cooled and deprotonated with triethyl amine then added it into the DMF solution of $Ni(OAc)_2.4H_2O$ (1mmol, 0.248g) and stirred for 2h. After 2h a methanol-water solution of Potassium para-phenyl diacrylate (K_2ppda) (1mmol, 0.262g) was added to the resulting green solution and stirred for an additional 1h. Green color single crystal suitable for X-ray diffraction was obtained by slow evaporation of the DMF solution after a few days. *Anal.*Calc. For C_{40} H_{58} Ni_2 N_4 O_{14} (936.32): C, 51.30% ; H, 6.24%; N, 5.98% Found: C,..... ; H,....; N, ...;O,.....; Cu,.....(%). IR (cm^{-1}):3200-3600 (br,vs), 2973 (vw), 1642 (vs), 1557 (vs),

1466 (s), 1413 (vs), 1371 (s), 1298 (vs), 1245 (w), 1194 (vw), 1149 (vw), 1078 (s), 1034 (vw), 984 (w), 880 (vw), 763 (vw), 711 (vw).

Synthesis of [{$Ni_2(L)_2(cinnamate)_2(H_2O)_2$}·DMF] (2).

The procedure was the same as that for complex **1**, except that a methanol-water solution of Potassium Cinnamate (2mmol, 0.358 g) was added instead of methanol-water solution of Potassium para-phenyl diacrylate. It was then filtered and the filtrate was kept in air. Green color single crystal suitable for X-ray diffraction was obtained by slow evaporation of DMF solution after a few days. *Anal.* Calc. For $C_{46}H_{60}Ni_2N_4O_{12}$ (978.40): C, 56.46%; H, 6.18%; N, 5.72% Found: C,..... ; H,....; N, ... IR (cm^{-1}): 3200-3600 (br,vs), 2979 (vw), 1641 (vs), 1550 (vs), 1467 (s), 1414 (vs), 1335 (w), 1301 (s), 1245 (w), 1192 (w), 1153 (w), 1108 (w), 1078 (s), 1035 (vw), 879 (vw), 761 (vw), 715 (vw), 684 (vw).

Crystallographic data collection and refinement

Data collections of complexes **1** and **2** were carried out at 120K on an Oxford Diffraction Gemini Ultra diffractometer. Cell refinement, indexing and scaling of the data sets were done with CrysAlisPro package, Version 1.171.35.10.[ref] The structures were solved by using the olex2.solve solution program[ref] using the charge flipping algorithm and refined by the full matrix least-squares method based on F^2 with all observed reflections.[ref] All calculations were performed using the WINGX.[ref] Packing diagrams were done with graphical program Diamond.[ref] Crystal data and details of refinements are given in Table 1.

Data collections of complexes **1** and **2** were carried out at 120K on an OxfordDiffraction Gemini Ultra diffractometer. Cell refinement, indexing and scaling of the data sets were done with CrysAlisPro package, Version 1.171.35.10 [ref, *Aligent (ed) (2010) CrysAlis PRO. Agilent Technologies Ltd, Yarnton*]. The structures were solved by using the olex2.solve solution program [ref, *Dolomanov OV, Bourhis L J, Gildea R J,*

Howard JAK, Puschmann H (2009) OLEX2: a complete structure solution, refinement and analysis program. J ApplCrystallogr 42: 339–341]

using the charge flipping algorithm and refined by the full matrix least-squares method based on F2 with all observed reflections [ref, *Sheldrick GM (2008) A short history of SHELX. ActaCrystallogr A64:112–122]*.All the calculations were performed using the WinGX.[ref]Packing diagrams were done with graphical programDiamond.[ref]Crystal data and details of refinements are given in Table 1.

Protein binding studies

We have studied the binding interactions of Ni(II) complexes with serum albumins (BSA/HSA) proteins using standard tryptophan fluorescence with excitation at 280 nm and the corresponding emission at 340 nm. Stock solutions of human serum albumin (HSA) and bovine serum albumin (BSA) were prepared in HEPES buffer (pH 7.2). The stock solutions of complexes were prepared by dissolving the complex in water. The absorption titration experiments were carried out by keeping the concentration of SA constant (9.6 µM for BSA; 6.05 µM for HSA) while varying the concentrations of Ni(II) complexes. The interactions of compounds with serum albumins were studied by recording the tryptophan fluorescence of HSA / BSA. To the solutions of serum albumin in HEPES buffer (pH 7.2) at room temperature, Ni(II) complexes were added, and the quenching of emission intensities at 340 nm (λ_{ex}, 280 nm) were recorded after gradual addition of 10 µL 0.3475 µM aqueous solution compounds. The Stern-Volmer constant (K_{sv}) and quenching rate constant (K_q) are calculated using the following two equations

$$F_0/F = 1 + K_{sv}[complex];\ K_{sv} = K_q\tau_0$$

Where F_0 and F are the fluorescence intensity in the absence and in the presence of the complex, and τ_0 is the lifetime of SA (~ 5×10^{-9} s). Whereas the following Scatchard equation have been used to calculate the binding constant (K_{bin}) and the number of binding sites (n).

$$\log[(F_o - F)/F] = \log K_{bin} + n \log[\text{complex}]$$

DNA binding studies

Electronic absorption spectral study

Electronic absorption spectral titration was carried out at a fixed concentration of complexes (5.69 µM) and gradually increasing the concentration of CT-DNA (0 to 25.42 µM). Intrinsic binding constant (K_{ib}) of the complex with CT-DNA was determined using the equation [ref]

$$\frac{[\text{DNA}]}{(\varepsilon_a - \varepsilon_f)} = \frac{[\text{DNA}]}{(\varepsilon_b - \varepsilon_f)} + \frac{1}{K_{ib}(\varepsilon_b - \varepsilon_f)}$$

Where [DNA] is the concentration of CT-DNA, ε_a is the extinction co-efficient value of the complex at a given CT-DNA concentration, ε_f and ε_b are the extinction co-efficient of the complex, in free solution and when fully bound to CT-DNA, respectively. The plot of [DNA]/($\varepsilon_a - \varepsilon_f$) vs [DNA] gives a straight line with $\frac{1}{(\varepsilon_b - \varepsilon_f)}$ and $\frac{1}{K_{ib}(\varepsilon_b - \varepsilon_f)}$ as slope and intercept, respectively. From the ratio of the slope to the intercept the value of K_{ib} was calculated.

Competitive binding fluorescence measurement

In order to examine whether the complexes could displace EB from their CT-DNA bound EB system, competitive studies of complexes with EB have been investigated with fluorescence spectroscopy. The competitive binding nature of EB and nickel (II) compounds with CT-DNA was investigated adopting fluorometric method using aqueous solution of EB bound CT-DNA in Tris-HCl buffer (P^H = 7.1) at room temperature. In presence of DNA, ethidium bromide (EB) exhibits fluorescence enhancement due to its intercalative binding to DNA. Competitive binding of nickel compound with CT-DNA results fluorescence quenching due to displacement of EB from CT-DNA. The fluorescence intensities at 602 nm (λ_{ex} = 500 nm) of EB bounded CT-DNA with

increasing concentration of Ni(II) complexes (0-6.81 µM) was recorded. The Stern-Volmer constant (K_{sv}) was calculated using Stern-Volmer equation [ref]

$$F_0/F = 1 + K_{sv}[complex]$$

Where F_0 and F are the emission intensity in absence and in presence of nickel (II) complexes, K_{sv} is the Stern-Volmer constant, and [complex] is the concentration of complexes.

Magnetic measurement

Temperature-dependent molar susceptibility measurements of polycrystalline samples were carried out at the *Servei de Magnetoquímica* of the *Centres Científics i Tecnològics* at the Universitat de Barcelona in a Quantum Design SQUID MPMSXL susceptometer with an applied field of 3000 and 198 G in the temperature ranges 2–300 and 2–30 K, respectively.

Results and discussion

Crystal structure description

The asymmetric unit of complex **1** and complex **2** are shown in Fig. 2 and Fig. 3. X-ray structural analysis of complexes revealed that complex **1** crystalizes in orthorhombic space group Pbca (No. 61) whereas complex **2** crystallizes in monoclinic space group P21/c (No. 14). The nickel atoms in both the complexes present identical distorted octahedral environments formed by a deprotonated Schiff base ligand, an oxygen atom from carboxylate, another oxygen atom from the other Schiff base via phenoxo bridged and a coordinated water molecule. The dinuclear unit is formed by two Ni(II) atoms, bridged by the two μ_2-phenoxo oxygen atoms. The selected bond lengths and bond angles are given in Table 2. The Ni-O bond lengths are varies from 2.021Å to 2.119Å for complex **1** and 2.030Å to 2.120Å for complex **2**, whereas Ni-N bond length is 2.020Å

and 2.015Å for complex **1** and complex **2** respectively, in good agreement with those observed for similar compounds in literature. The distance between two nickel atoms is 3.105Å for both the complexes, indicating the absence of any bond between two nickel centers. The largest bond angle in **1** and **2** are O(3)-Ni(1)-O(5) [172.03(10)], and O(3) - Ni(1)-O(4) [172.48(6)] whereas smallest bond angle in **1** and **2** are O(3)-Ni(1)-N(1) [79.93(12)°] and O(4) - Ni(1)- N(1) [80.83(8)°]. The Ni-O-Ni bridge angles are 98.14Å and 97.88Å for complex **1** and complex **2** respectively. A rather unusual feature of both the complexes is the *fac* configuration of the Schiff base ligand. There are several reports [ref] of a double phenoxo-bridged Ni(II) dimer with tridentate ligands, but in most of them, the ligands are coordinated in a *mer* configuration.

Electronic absorption and emission spectra of Ligand

The electronic absorption spectra of HL (0.98 μM) exhibits three sharp bands at 215 nm (ε ~1.78×10^5 liter mole^{-1} cm^{-1}), 254 nm (ε ~0.89×10^5 liter mole^{-1} cm^{-1}), and 312 nm (ε ~0.26×10^5 liter mole^{-1} cm^{-1}) and two relatively weak band at 278 nm (ε ~0.26×10^5 liter mole^{-1} cm^{-1}) and 400 nm (ε ~0.09×10^5 liter mole^{-1} cm^{-1}) (Fig. 1S). On excitation at 254 nm HL exhibits luminescence at 275 nm, 312 nm, 355 nm and 371 nm with a fluorescence quantum yield Φ_s= 0.295 (Fig. 2S). The positions of emission bands remain unchanged when λ_{ex} is varied between (λ_{ex} - 10) and (λ_{ex} + 10) nm.

Electronic absorption and emission spectra of complexes

An electronic spectrum of 10^{-6} M aqueous solution of complexes is shown in Fig. 3 Complex **1**, exhibits bands at 217 nm (1.674×10^5 liter mole^{-1} cm^{-1}), 277 nm (0.752×10^5 liter mole^{-1} cm^{-1}), 313 nm (1.226×10^5 liter mole^{-1} cm^{-1}) and 363 nm (0.188×10^5 liter mole^{-1} cm^{-1}). Whereas complex **2** exhibits bands at 244 nm (0.365×10^5 liter mole^{-1} cm^{-1}), 273 nm (0.611×10^5 liter mole^{-1} cm^{-1}) and 393 nm (0.103×10^5 liter mole^{-1} cm^{-1}). Both the complexes exhibit red shifted emission with a large

Stokes shift. On excitation at 313 nm complex **1** exhibits luminescence bands at 434, 465 and 535 nm with a fluorescence quantum yield Φ_s= 0.47. For **2**, λ_{ex}, 273 nm; λ_{em}, 313, 382, 441, 535 nm and Φ_s= 0.49. The positions of emission bands remain unchanged when λ_{ex} is varied between (λ_{ex} - 10) and (λ_{ex} + 10) nm. Detailed spectral data of complexes are summarized in Table 3

ESI mass spectrometry

ESI mass spectra (Fig. 7S) of HL were recorded in methanol. The ESI mass spectrometric data of HL shows a peak at m/z = 194.25, which corresponds to $[C_{11}H_{15}NO_2+ H]^+$ mono cation, confirm the chemical composition of ligand. This observation evidence that the chemical composition of HL in methanol solution is same as detected in solid state.

IR spectral results

IR spectra of complex **1** and **2** are shown in Fig. 3S and Fig. 4S, and the most important absorption bands are summarized in the experimental section and in Table 1S. IR spectra show that ν(O-H) stretching vibration appear in the region 3200-3600 cm^{-1}. Stretching vibrations in the region 2973 – 2992 cm^{-1} are for C_{sp2}–H bond and bands at 2939 – 2941 cm^{-1} are for C_{sp3}–H bond. A strong and sharp band due to asymmetric stretching bands of carboxylate appear at 1642 cm^{-1} for complex **1** and 1641 cm^{-1} for complex **2**. Whereas symmetric stretching band for the carboxylate is observed at 1414 cm^{-1} for complex **1** and 1413 cm^{-1} for complex **2** respectively. Aromatic ν(C=C) and aliphatic ν(C=N) stretching vibrations appears in the region 1466 - 1550 cm^{-1} (for **1**) and 1467-1557 cm^{-1} (for **2**). $\nu_s(C\text{-}O)_{phenolic}$ stretching vibration appears at 1245 for both the complex.

Protein Binding Studies

Fluorescence spectroscopic studies

It is well-known that the transport of drugs through the bloodstream is affected via the interaction of drugs with blood plasma proteins, mostly with serum albumin. The serum albumins are the most abundant proteins in the circulation system and play important roles in the delivery of many pharmaceuticals to the sites of diseases [ref]. It is therefore important to study the interactions of biologically active compounds with these transport proteins since binding to these proteins may lead to loss or enhancement of the biological properties of the original drug, or provide paths for drug transportation. Interactions of metallodrugs with proteins are crucial for their bio-distribution, toxicity, and even for their mechanism of action. The solutions of human serum albumin (HSA, bearing one tryptophan, Trp-214) and its extensively studied homologue bovine serum albumin (BSA, with two tryptophan, Trp-134 and Trp-212) exhibit an intense fluorescence emission when excited at 280 nm. The interactions of complexes **1** and **2** with serum albumins (BSA/HSA) have been studied from the binding experiments. The binding of serum albumins with the complexes were studied by fluorescence measurement at room temperature. Various concentrations of complexes (0-6.81 µM) were added to the solutions of BSA (9.6 µM) and HSA (6.05 µM) and the fluorescence spectra were recorded in the range 290-450 nm upon excitation at 280 nm. The effect of the complexes on the fluorescence emission spectrum of BSA and HSA are given in the Fig. 4 and Fig. 5 respectively upon the addition of the complex **1** and **2** to the solution of BSA and HSA a significance decrease of the fluorescence intensity (at 340 nm up to 56.5% and 77.51% from the initial fluorescence intensity of BSA has been observed whereas for HSA these are 49.98 and 75.71%) which is usually attributed to subunit association, protein denaturation, substrate binding or conformational changes of the protein (ref). The significant fluorescence emission quenching as a result of the addition of complexes to the BSA fluorescence signal at 340 nm as well as to the HSA fluorescence maximum at 330 nm indicates the binding of each complex to the albumin may

be attributed to changes in tryptophan environment of SA because of possible change in protein secondary structure (ref). The calculated quenching constant, K_q ($>10^{12}$ M^{-1} s^{-1}) is higher than diverse kinds of quenchers for biopolymer fluorescence (2×10^{10} M^{-1} s^{-1}) indicating the existence of a static quenching mechanism. [ref] If it is assumed that the binding of compounds with BSA and HSA occurs at equilibrium, the association binding constant (K_{bin}) can be analyzed according to the Scatchard equation $\log[(F_o - F)/F] = \log K_{bin} + n \log[\text{complex}]$ where K_{bin} is the binding constant of the compound with SA and n is the number of binding sites. The binding constant (K_{bin}) and the number of binding sites (n) have been calculated from the plot of log $[(F_o - F)/F]$ versus log [complex] (Fig. 6). The value of Stern-Volmer constant (K_{sv}), quenching rate constant (K_q), binding constant (K_{bin}) and the number of binding sites per albumin (n) for the complexes are given in Table 4. The calculated value of n is around 1 for both the complexes, indicating the existence of just a single binding site in SA for both the complexes. However, the results showed that complex **2** interacts with SA more strongly than the **1**.

The value of the association constant of compound to albumin should be in such a range that allows possible binding to, transfer by, and release from the albumins at its biological target. It should be noted that the binding constants of the complexes are lying in such a promising range. The values of binding constants are high enough (1.39×10^5 to 3.89×10^5 M^{-1}), revealing the affinity of the complexes to bind to albumins; they are quite lower than the association constant of avidin to diverse ligands ($K_{bin} \sim 10^{15}$ M^{-1}), which is among the strongest known noncovalent interactions, revealing the possibility of release upon arrival to target tissues or cells [ref].

Absorption spectral studies

Generally, quenching occurs through either dynamic or static quenching. The dynamic quenching is a process in which the fluorophore and the quencher come into contact during the transient existence of the excited state, whereas static quenching refers to the formation of fluorophore-quencher complex in the ground state. The easiest method to determine the type of quenching is UV−visible absorption spectroscopy. Fig. 7 and Fig. 8 show the UV−visible spectra of SA in the absence and presence of the complexes, which indicated that the absorption intensity of SA was enhanced as the complexes were added. There was a little red shift of about 1 nm for BSA and 2 nm for HSA upon addition of complex **1** whereas upon addition of complex **2** little blue shift of about 2 nm and 3 nm occurs for BSA and HSA respectively. It revealed the existence of a static interaction between SA and the tested complexes. The apparent association constant (K_{app}) were calculated using the following equation.

$$\frac{1}{(A_{obs} - A_0)} = \frac{1}{(A_c - A_0)} + \frac{1}{K_{app}(A_c - A_0)}$$

The values of apparent association constant (K_{app}) were depicted in Table 5.

DNA binding studies

DNA binding is an importance footstep for chemical nuclease activity of the metal complexes. Therefore before evaluating the potential of another bio-activities of the new complexes, the interaction between DNA and the new synthesized compounds was examined. The mode and tendency for the binding of complexes to CT-DNA were studied with different methods.

Absorption spectral studies

Electronic absorption spectroscopy is one of the most common techniques used for investigating the mode of binding between the metal complexes and DNA [ref]. In general the metal complexes

binding to DNA through intercalation results in hypochromism with or without a small red or blue shift, since the intercalative mode involves in a strong stacking interaction between the planer aromatic chromophore and the base pairs of DNA [ref].

Absorption titration experiments were performed with fixed concentrations of Ni(II) complexes while gradually increasing the concentrations of CT-DNA (0-25.42µM) at room temperature in Tris-HCl buffer (P^H = 7.1). The representative absorption spectra of the complexes in the absence and presence of CT-DNA are shown in Fig. 9 Complex **1** exhibited hypochromism of about 13% at 313 nm, 30% at 395 nm whereas exhibit hyperchromism of about 23% at 277 nm. A new band appeared at 257 nm. On the other hand complex **2** also exhibited hypochromism of about 60% at 393 nm and hyperchromism of about 37.72% at 273 nm. About 8 nm blue shift occurs at 273 nm. However, complex **2** showed more hypochromicity when compared to that of complex **1**, indicating that the binding strength of complex **2** is much stronger than that of complex **1**. To further compare the binding ability of the nickel complexes, their intrinsic binding constant (K_{ib}) were determined from the following equation [ref]

$$\frac{[DNA]}{(\varepsilon_a - \varepsilon_f)} = \frac{[DNA]}{(\varepsilon_b - \varepsilon_f)} + \frac{1}{K_{ib}(\varepsilon_b - \varepsilon_f)}$$

Where [DNA] is the concentration of DNA in the base pairs, ε_a is the apparent absorption coefficient corresponding to A_{obs}/[compound], ε_f is the extinction coefficient of the free compound, and ε_b is the extinction coefficient of the compound when fully bound to DNA. From the plot of [DNA]/ (ε_a-ε_f) versus [DNA] (inset of fig. 9), the intrinsic binding constant (K_{ib}) was calculated from the ratio of the slope and the intercept. The magnitude of intrinsic binding constant (K_{ib}) were calculated to be 3.43×10^5 and 3.9×10^5 M^{-1} for complex **1** and complex **2** respectively. These results

indicate that both the new nickel complexes bind to the DNA helix via intercalation. The above observations were comparable to those reported earlier for various metallointercalators [ref].

Competitive binding between Ethidium Bromide and Compounds

Furthermore, the proof for the binding of the complexes **1** and **2** to CT-DNA via intercalation were demonstrated through the emission quenching experiment. EB is a planer, cationic dye, and one of the most sensitive fluorescence probes which can bind to DNA through intercalation [ref]. The emission spectra of CT-DNA bound EB in the absence and presence of complexes were given in Fig. 10. Due to the displacement of EB from DNA sequence by a quencher, fluorescence intensity decreases as the number of binding sites on the DNA that is available to the EB also reduced, which is the fundament of displacement technique.

On adding Ni(II) complexes (0-6.81 µM) to EB (5 µM) bounded CT-DNA (8.47 µM) the quenching in the emission of EB bounded CT-DNA takes place. The emission band exhibited hypochromism up to 54.44% and 81.87% of the initial fluorescence intensity for complex **1** and complex **2** respectively. It suggested that the ethidium bromide molecules are displaced from the CT-DNA binding sites by complexes under investigation. Quenching parameters were analyzed following the Stern-Volmer equation.

$$F_0/F = 1 + K_{sv}[\text{complex}]$$

K_{sv} values for complex **1** and complex **2** are 1.755×10^5 and $4.698 \times 10^5\ M^{-1}$.

Further, the apparent DNA binding constant (K_{app}) values were also calculated using the equation

$$K_{EB}[EB] = K_{app}[\text{complex}]$$

Where the complex concentration is the value at a 50% reduction in the fluorescence intensity of EB, K_{EB} (1.0×10^7 M^{-1}) is the DNA binding constant of EB, [EB] is the concentration of EB = 5 μM), and they are given in Table 6. From these observed data, it is seen that complex **2** has more binding affinities than the complex **1** which is in agreement with the results observed from the electronic absorption spectra. Moreover the experimental quenching constants and binding constants of the nickel(II) complexes suggest that the interaction of complexes with CT-DNA should be of intercalation [ref].

Magnetic properties of complexes

Temperature-dependent magnetic susceptibility measurements on polycrystalline samples of complexes **1** and **2** were carried out in the temperature range 1.9-300 K. The plot of $\chi_M T$ versus T for the two complexes is shown in Figure AF1, where χ_M is the molar magnetic susceptibility and T is the absolute temperature. The $\chi_M T$ value measured at room temperature of 2.33 and 2.28 cm^3Kmol^{-1} is slightly higher than the expected value for two uncoupled S = 1 spins assuming g = 2 (2.00 cm^3Kmol^{-1}). Upon cooling, $\chi_M T$ varies smoothly in both cases and finally decreases abruptly below 50 K and 100 K in complexes **1** and **2**, respectively.

The behaviour displayed by complexes **1** and **2** confirms the presence of an overall antiferromagnetic interaction in the system. The experimental magnetic data were simulated with the MAGPACK program. ref needed: (a) J.J.Borràs-Almenar, J. M. Clemente-Juan, E. Coronado and B.S.Tsukerblat, J. Comput. Chem., 2001, 22, 985; (b) J.J.Borràs-Almenar, J. M. Clement-Juan, E. Coronado and B. S. Tsukerblat, Inorg. Chem., 1999, 38, 6081. Due to the crystallographic equivalence of both Ni(II) ions in the asymmetric dinuclear unit of each complex, the magnetic model considered one single g value for each compound. Additionally, the interaction between Ni_2

dinuclear units through the ppda bridge in **2** was neglected due to the long interdinuclear distances of 13 Å. (refs: a) Q. Sun, Q. Yue, J.-Y. Zhang, L. Wang, X. Li, E.-Q. Gao, *Cryst. Growth Des.* **2009**, *9*, 2310-2317; b) Q. Sun, A.-l. Cheng, Y.-Q. Wang, Y. Ma, E.-Q. Gao, *Inorg. Chem.* **2011**, *50*, 8144-8152) Consequently, both complexes **1** and **2** can be magnetically treated as homodinuclear Ni(II) systems, and their magnetic behavior studied with the Hamiltonian $H = -JS_1S_2$, $S_1 = S_2 = S_{Ni}$. A good agreement between experimental and simulated curves was found by using the following parameters: $g_{Ni} = 2.15$, $D_{Ni} = 4.0$ cm^{-1} and $J_{Ni\text{-}Ni} = -0.60$ cm^{-1} for **1** and $g_{Ni} = 2.15$, $D_{Ni} = 4.8$ cm^{-1} and $J_{Ni\text{-}Ni} = -3$ cm^{-1} for **2**. Temperature-independent paramagnetism (TIP) was considered equal to 200×10^{-6} cm^{3}mol^{-1}. The simulated curves are represented together with the experimental ones in Figure AF1.

Within the asymmetric dinuclear units of complexes **1** and **2**, the phenoxido bridge of the Schiff base ligand works as the only magnetic exchange pathway available between Ni(II) ions. The major factor controlling the magnetic coupling ($J_{Ni\text{-}Ni}$) in this type of compounds is the phenoxido-based Ni-O-Ni angle. From experimental and theoretical data, it was concluded that an antiferromagnetic coupling should be expected for phenoxido-bridged dinuclear Ni(II) complexes showing a Ni-O-Ni angle larger than 93-96°, being the $J_{Ni\text{-}Ni}$ constant more negative with increasing Ni-O-Ni angle. (ref. needed: a) X.-H. Bu, M. Du, L. Zhang, D.-Z. Liao, J.-K. Tang, R.-H. Zhang, M. Shionoya, *J. Chem. Soc., Dalton Trans.*, **2001**, 593-598; b) A. Burkhardt, E. T. Spielberg, S. Simon, H. Gçrls, A. Buchholz, W. Plass, *Chem. Eur. J.* **2009**, *15*, 1261-1271; c) R. Biswas, S. Giri, S. K. Saha, A. Ghosh, *Eur. J. Inorg. Chem.* **2012**, 2916-2927) In the current compounds, this angle shows values of 98.14° and 97.88° for complexes **1** and **2**, respectively, that is slightly above the previously mentioned crossover angle. Thus, the weak antiferromagnetic

constants found by simulation of the data in both compounds are in complete agreement with the well-established magnetostructural correlation.

Conclusion

We have presented here the synthesis, characterization and photo physical studies of N, O, O donors tridentate ligand. Two octahedral Ni(II) complexes have been synthesized using these ligand and characterized by various spectral techniques. The molecular structures of complexes have been confirmed by single-crystal X-ray diffraction studies. The DNA binding results showed that both the complexes bind with DNA via intercalation. In addition the interaction properties with proteins of the new complexes were studied by UV-visible and fluorescence spectroscopies, and the results indicated that the complex **2** has resulted in strong binding compared with the complex **1**. The magnetic behavior of complexes **1** and **2** can be understood in the light of a Ni(II) homodinuclear model. As expected from their structural features, both complexes show very weak antiferromagnetic coupling between phenoxido-bridged Ni(II) ions, in agreement with previously established magnetostructural correlations.

Acknowledgements

The authors gratefully acknowledge the financial assistance given by the CSIR, Government of India, to Dr. Subal Chandra Manna (Project No. 01 (2743)/13/EMR-II). A.F acknowledges financial support from the Spanish Ministerio de Economía y Competitividad (MINECO) through CTQ2012-32247 and for a Ramón y Cajal Fellowship (RYC-2010-05821), and from the regional Generalitat de Catalunya authority (2014SGR-129).

Supplementary information

…….. and …… contain the supplementary crystallographic data for **1** and **2** respectively. These data can be obtained free of charge via http://www.ccdc.cam.ac.uk/conts/retrieving.html, or from the Cambridge Crystallographic Data Centre, 12 Union Road, Cambridge CB2 1EZ, UK; fax: (+44) 1223-336-033; or e-mail: deposit@ccdc.cam.ac.uk. Figures showing IR, electronic and fluorescence spectra are provided as supporting information.

References ……..

Table 1. Crystal Data and Structure Refinement for compounds **1** and **2**

Complex	**1 (ICVU-252)**	**2 (ICVU-231)**
Empirical formula	C_{40} H_{58} Ni_2 N_4 O_{14}	C_{46} H_{60} Ni_2 N_4
Formula mass, g mol^{-1}	936.32	978.40
Crystal system	Orthorhombic	Monoclinic
Space group	*Pbca*	*P21/c*
a, Å	15.8130(4)	12.6288(2)
b, Å	16.5253(4)	16.0777(2)
c, Å	16.8416(4)	12.8996(2)
α ,deg	90	90
β, deg	90	115.544(2)
γ, deg	90	90
V, $Å^3$	4400.96(19)	2363.15(7)
Z	4	2
$D_{(calcd)}$, g cm^{-3}	1.413	1.375
μ(Mo-Kα), mm^{-1}	0.924	0.861
F(000)	1976	1032
Theta range, deg	2.2-27.5	3.1- 27.5
No. of collcd data	34385	47065
No. of unique data	5055	5428
R_{int}	0.068	0.036
Observed reflections [$I > 2\sigma(I)$]	3704	5242
Goodness of fit (F^2)	1.044	1.288
Parameters refined	358	305
*R*1 [$I > 2\sigma(I)$] [a]	0.0545	0.0379

wR2 [*I*> 2σ(*I*)] [a]	0.1369	0.0840
Residuals, e Å^{-3}	-0.43, 0.96	-0.47, 0.47

[a]$R1(Fo) = \Sigma \left| \left| Fo \right| - \left| Fc \right| \right| / \Sigma \left| Fo \right|$, $wR2(Fo^2) = [\Sigma w (Fo^2 - Fc^2)^2 / \Sigma w (Fo^2)^2]^{1/2}$

Table 2. Selected bond distances (Å) and angles (°) for complexes

Bond lengths	Complex **1**		Complex **2**
Ni(1)-O(1)	2.082(2)	Ni(1)-O(1)	2.0600(17)
Ni(1)-O(3)	2.119(3)	Ni(1)-O(1W)	2.1003(16)
Ni(1)-O(4)	2.074(2)	Ni(1)-O(3)	2.0306(16)
Ni(1)-O(5)	2.021(2)	Ni(1)-O(4)	2.1203(17)
Ni(1)-N(1)	2.020(3)	Ni(1)-N(1)	2.015(2)
Ni(1)-O(5_a)	2.088(2)	Ni(1)-O(3_a)	2.0874(15)
Bond angles			
O(1)- Ni(1)-O(3)	91.56(10)	O(1)-Ni(1)-O(1W)	170.76(6)
O(1)-Ni(1)-O(4)	171.18(9)	O(1)- Ni(1)-O(3)	88.56(6)
O(1)-Ni(1)-O(5)	90.52(9)	O(1)- Ni(1)-O(4)	90.49(7)
O(1)- Ni(1)-N(1)	99.55(11)	O(1)- Ni(1)- N(1)	97.41(8)
O(1)-Ni(1)-O(5_a)	86.17(9)	O(1)- Ni(1)-O(3_a)	87.86(6)
O(3)-Ni(1)-O(4)	93.42(10)	O(1W)- Ni(1)-O(3)	88.64(6)
O(3)-Ni(1)-O(5)	172.03(10)	O(1W)- Ni(1)-O(4)	93.41(6)
O(3)-Ni(1)-N(1)	79.93(12)	O(1W)- Ni(1)- N(1)	91.49(8)
O(3)-Ni(1)-O(5_a)	105.95(10)	O(1W) - Ni(1)-O(3_a)	83.03(6)
O(4)-Ni(1)-O(5)	85.53(9)	O(3) - Ni(1)-O(4)	172.48(6)
O(4)-Ni(1)-N(1)	88.50(11)	O(3) - Ni(1)- N(1)	91.90(8)
O(4)-Ni(1)-O(5_a)	85.46(9)	O(3) - Ni(1)-O(3_a)	82.12(6)
O(5)-Ni(1)-N(1)	92.13(11)	O(4) - Ni(1)- N(1)	80.83(8)
O(5)-Ni(1)-O(5_a)	81.86(8)	O(3_a)- Ni(1)-O(4)	105.30(6)
O(5_a)-Ni(1)-N(1)	171.79(11)	O(3_a)- Ni(1)-N(1)	171.96(9)

Table 3. Electronic absorption and emission spectra of HL and complexes

	Absorption / λ (nm); ε (M^{-1} cm^{-1})	Emission (nm)	Δν[a], nm	ϕ
HL	215 (1.78×10^5), **254** (0.89×10^5), 278 (0.26×10^5), 312 (0.26×10^5), 400 (0.09×10^5)	275, 312, 355, 371	21, 58, 101, 117	0.295
1	217 (1.674×10^5), 277 (0.752×10^5), **313** (1.226×10^5), 363 (0.188×10^5), 395 (0.140×10^5)	434, 465, 535	121, 152, 222	0.47
2	244 (0.365×10^5), **273** (0.611×10^5), 393 (0.103×10^5)	313, 382, 441, 535	40, 109, 168, 262	0.49

Bold number indicates the excitation wavelengths. [a]Stoke shift

Table 4. Quenching Constant (K_q), Binding Constant (K_{bin}) and number of Binding Sites (n) for the Interactions of Complexes with BSA and HSA

	Complexes	K_{sv} (M^{-1})	K_q ($M^{-1}s^{-1}$)	K_{bin} (M^{-1})	n

BSA	**1**	1.765×10^{5}	3.53×10^{13}	1.39×10^{5}	0.93
	2	3.56×10^{5}	7.12×10^{13}	1.78×10^{5}	1.43
HSA	**1**	1.35×10^{5}	2.70×10^{13}	2.09×10^{5}	0.76
	2	4.50×10^{5}	9.00×10^{13}	3.89×10^{5}	1.05

Table 5. The values of apparent association constant (K_{app}) of complexes

Complex **1**		Complex **2**	
Serum Albumins	K_{app} (M^{-1})	Serum Albumins	K_{app} (M^{-1})
BSA	6.11×10^{4}	BSA	7.06×10^{4}
HSA	1.85×10^{4}	HSA	2.56×10^{4}

Table 6. Emission spectral properties of the Ni(II) complexes bound to CT-DNA

Complexes	λ_{max} (nm)	change in emission	Δε (%)	K_{sv} (M^{-1})	K_{app} (M^{-1})
1	602	hypochromism	54.44	1.755×10^{5}	8.78×10^{6}
2	602	hypochromism	81.87	4.698×10^{5}	14.53×10^{6}

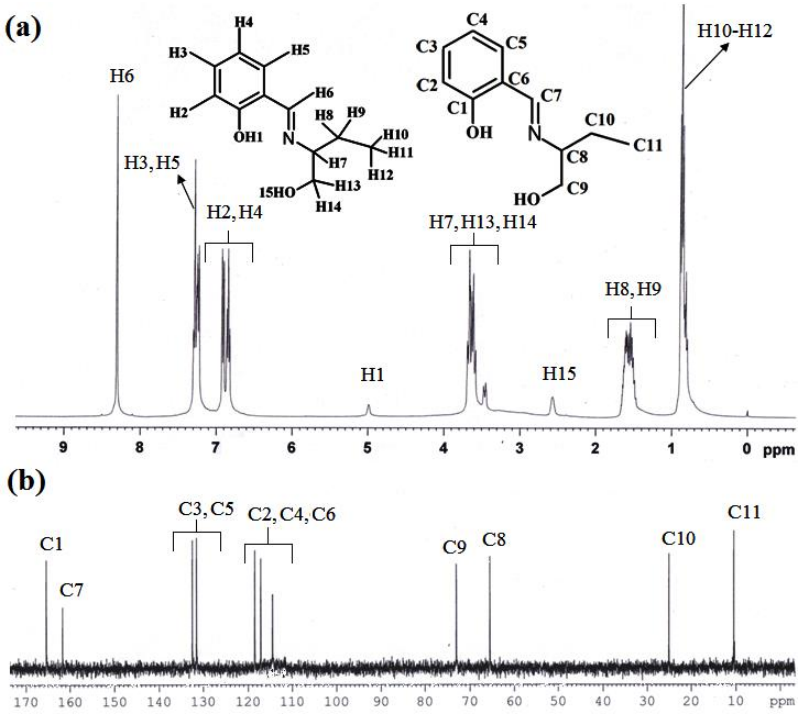

Fig. 1. ^{1}H (**a**) and ^{13}C NMR (**b**) spectra of HL.

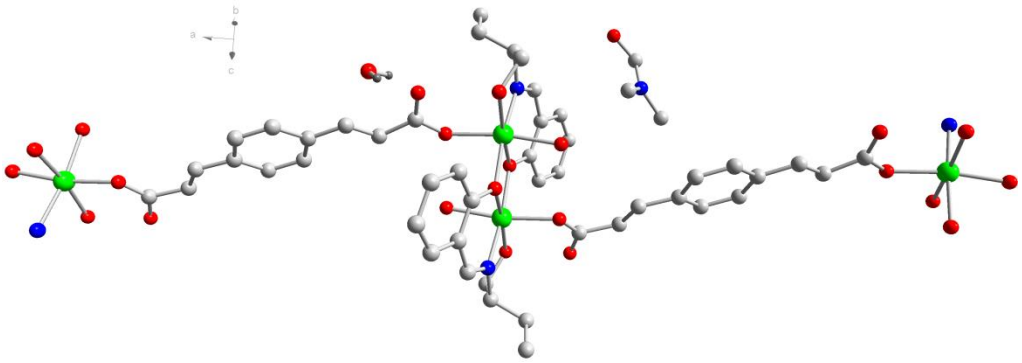

Fig. 2. Repeating unit of complex **1**

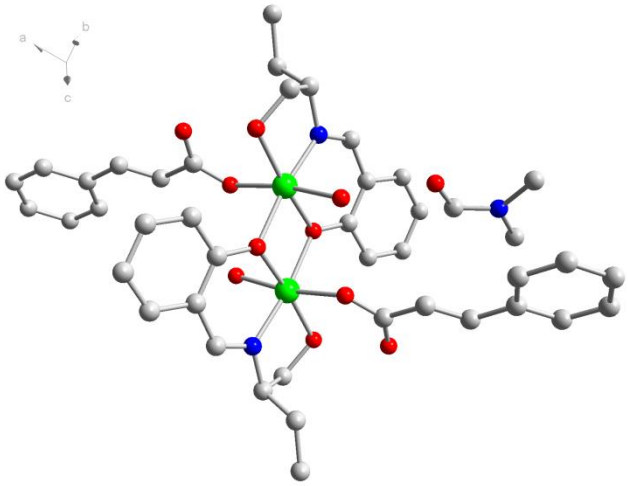

Fig. 3. Asymmetric unit of complex **2**

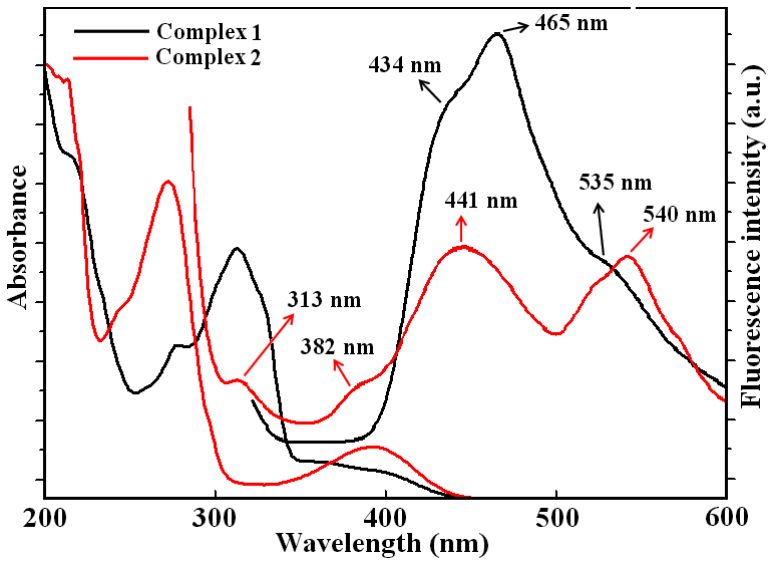

Fig. 3. Absorption (left) and fluorescence (right) spectra of complex **1** and **2**. (λ_{ex} = 273 nm and 313 nm for 1 and 2 respectively. Excitation and emission slit width = 5 nm).

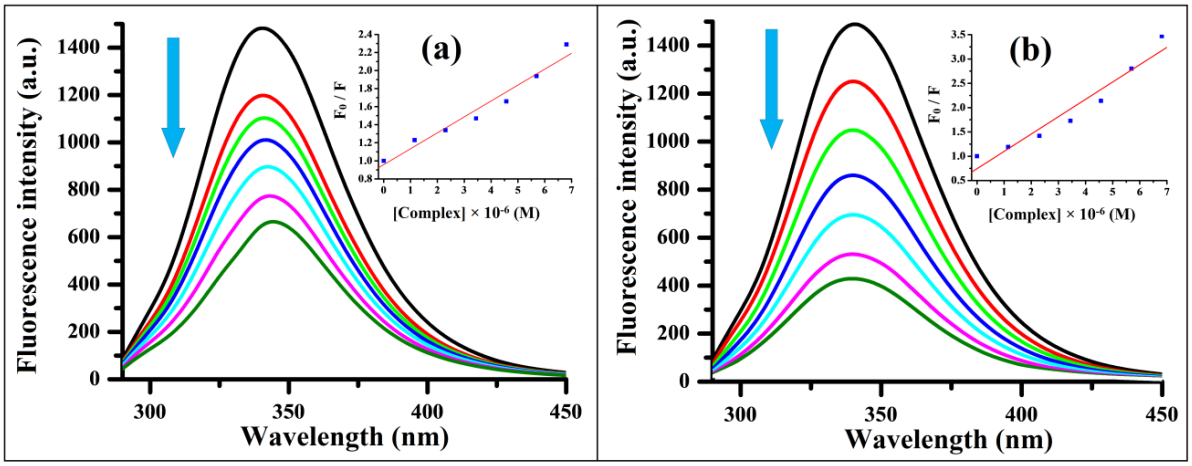

Fig. 4. Emission spectrum of BSA (λ_{ex} = 280 nm; λ_{em} = 340 nm) in the presence of increasing amounts of complexes **1** (a), 2 (b) (0−6.81 μM). Arrow shows that the emission intensity changes upon increasing complex concentration.

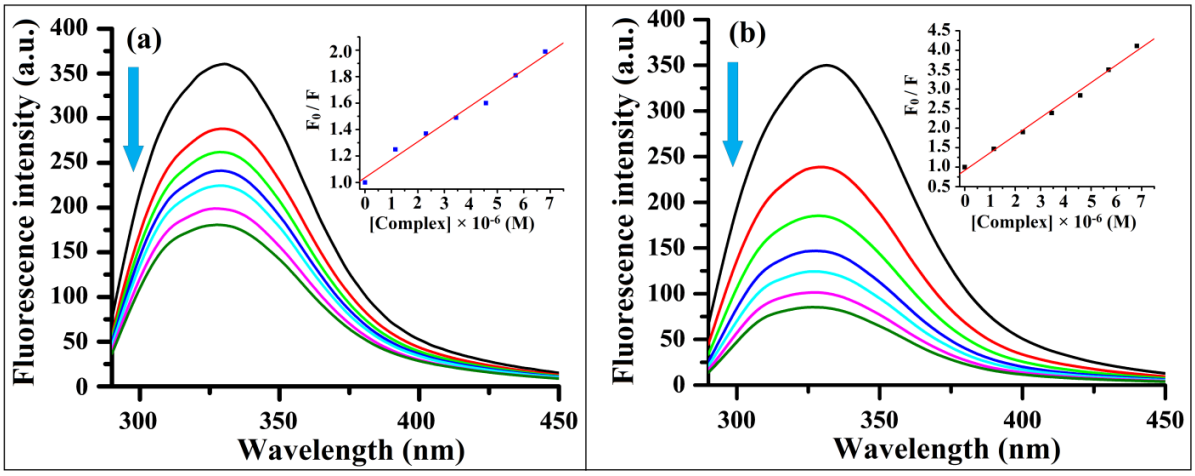

Fig. 5. Emission spectrum of HSA (λ_{ex} = 280 nm; λ_{em} = 340 nm) in the presence of increasing amounts of complexes 1 (a), 2 (b) (0−6.81 μM). Arrow shows that the emission intensity changes upon increasing complex concentration

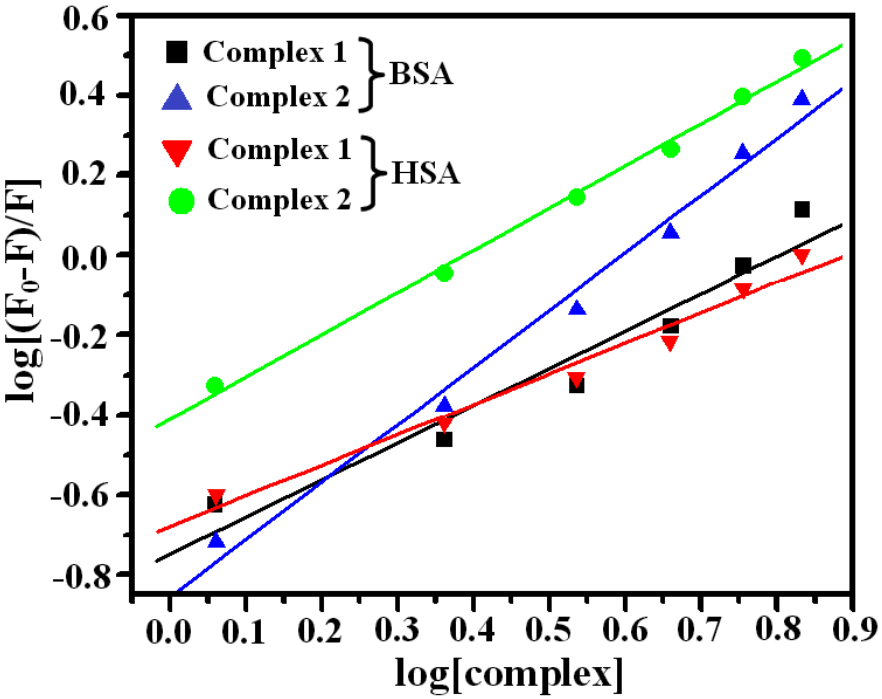

Fig. 6. Scatchard plot of the SA fluorescence titration for complexes

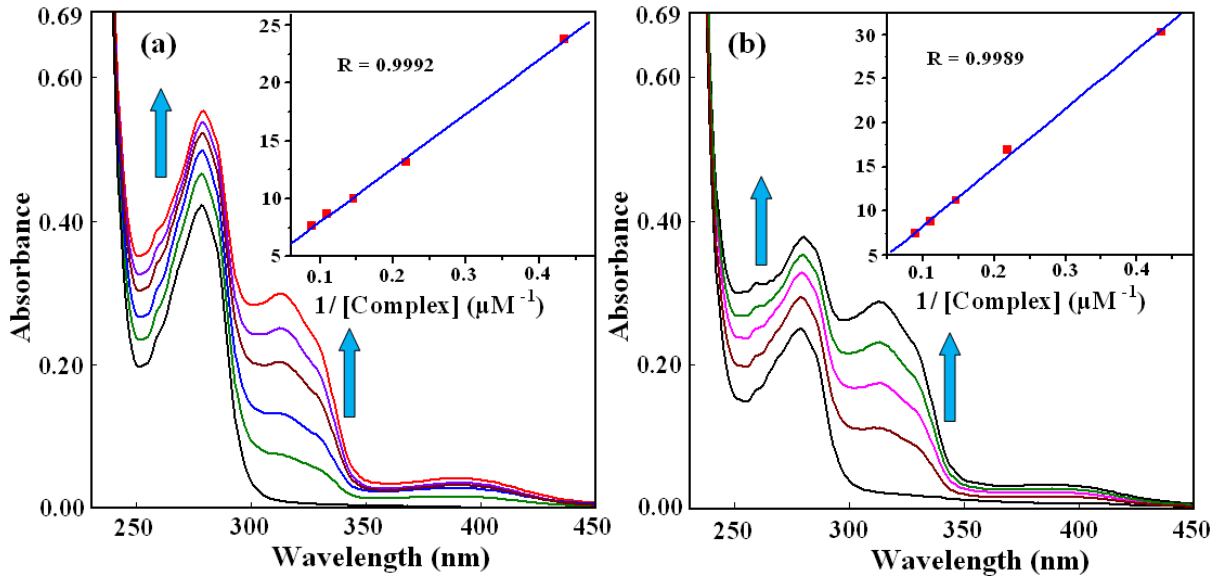

Fig. 7. UV-Vis absorption spectra of (a) BSA and (b) HSA upon gradual addition of 20 µl 0.3475 µM aqueous solution of complex **1** at room temperature.

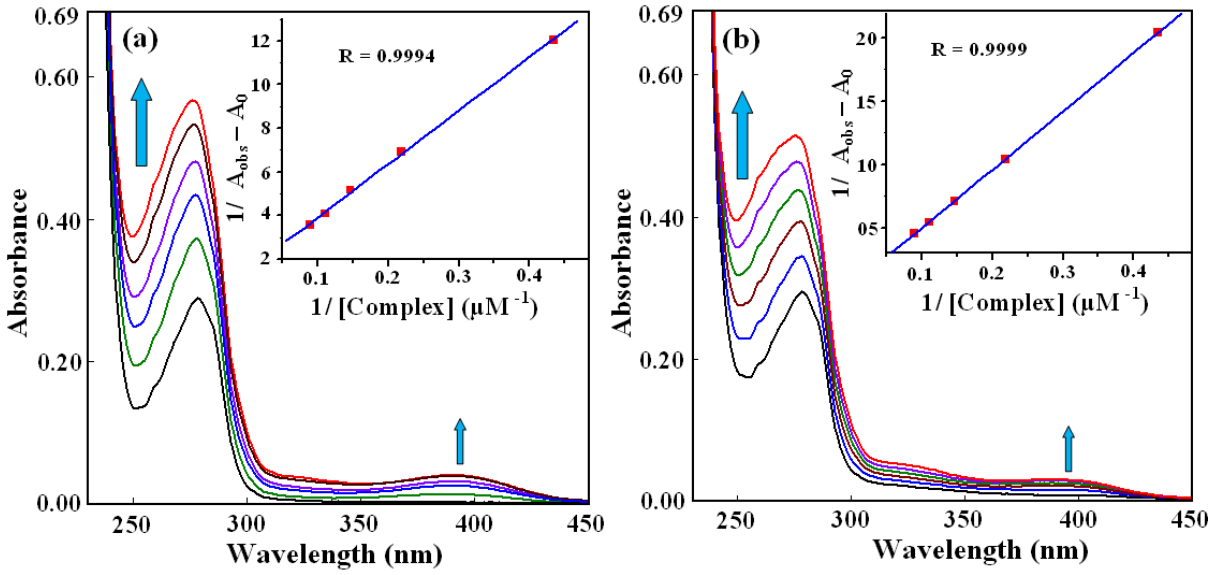

Fig. 8. UV-Vis absorption spectra of (a) BSA and (b) HSA upon gradual addition of 20 µl 0.3475 µM aqueous solution of complex **2** at room temperature.

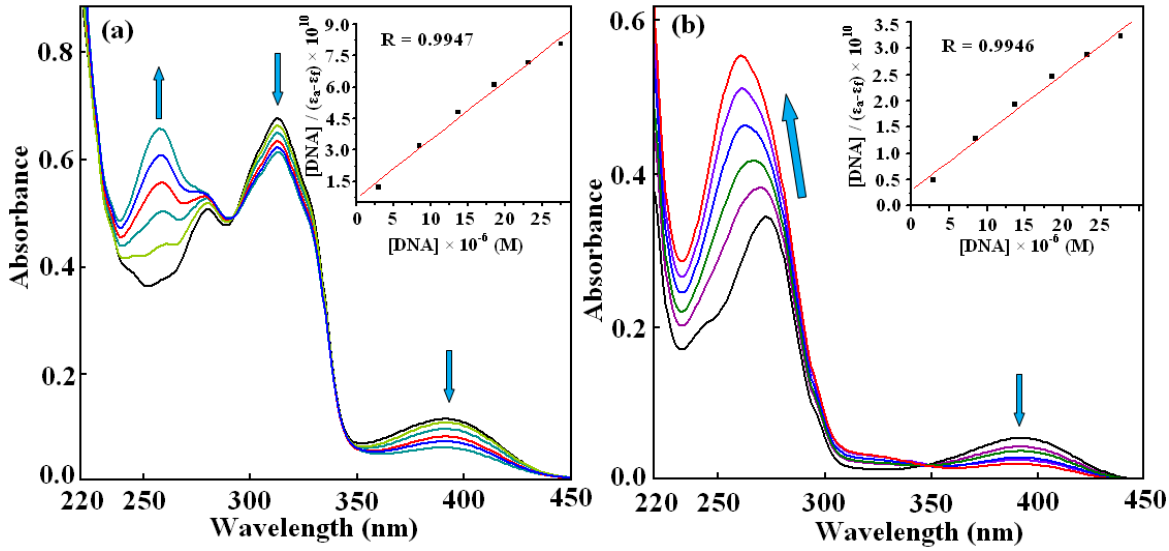

Fig. 9. Absorption titration spectra of complexes **1** (a) and **2** (b) in the absence (black line) and presence (other lines) of CT-DNA to complex at room temperature. Inset: Plot of [DNA]/(ε_a-ε_f) versus [DNA]. Arrow shows the absorbance changes upon increasing CT-DNA concentration

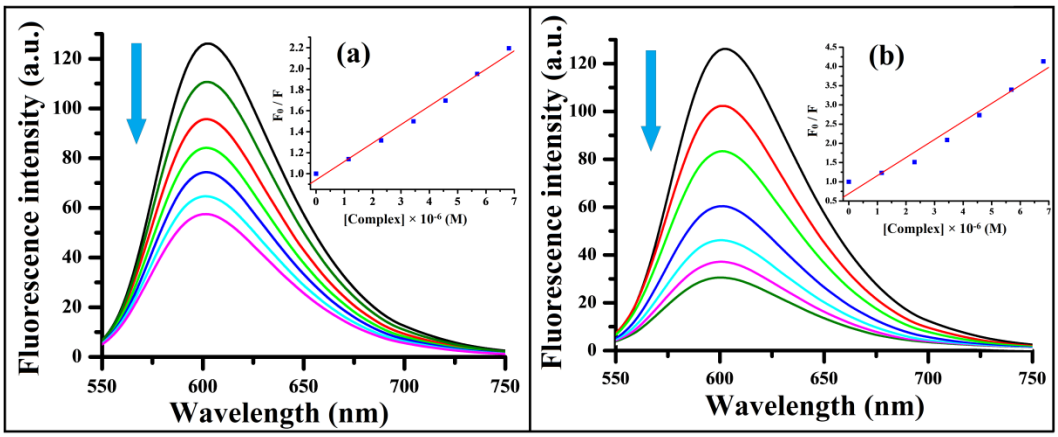

Fig. 10. Emission spectra of EB bounded CT-DNA in the presence of complex **1** (a) and complex **2** (b). Inset: Stern-Volmer plot of fluorescence titrations.

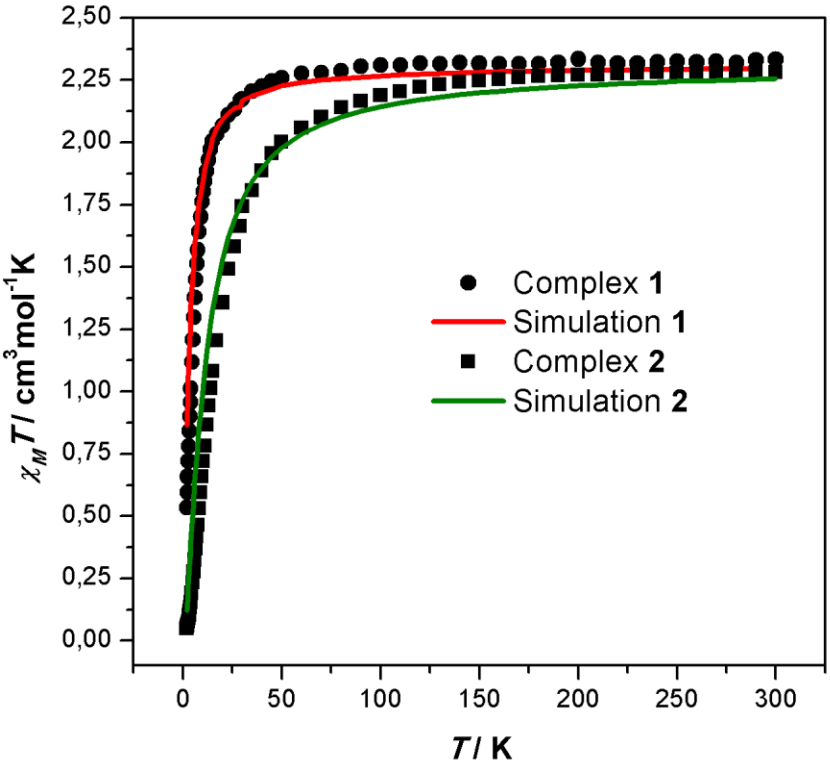

Figure AF1. Thermal dependence of the $\chi_M T$ for complexes **1** and **2**. The straight lines the simulations obtained considering a Ni(II) homodinuclear magnetic model and using the parameters mentioned in the text.